Hindawi
International Journal of Photoenergy
Volume 2018, Article ID 1678385, 16 pages
https://doi.org/10.1155/2018/1678385

Research Article

Modelling and Simulation of the Radiant Field in an Annular Heterogeneous Photoreactor Using a Four-Flux Model

O. Alvarado-Rolon,[1] R. Natividad,[2] R. Romero,[2] L. Hurtado,[2] and A. Ramírez-Serrano[1]

[1]*Facultad de Química, Universidad Autónoma del Estado de México, Paseo Colon esq. Paseo Tollocan s/n, 50120 Toluca, MEX, Mexico*
[2]*Facultad de Química, Centro Conjunto de Investigación en Química Sustentable UAEM-UNAM, Universidad Autónoma del Estado de México, Carretera Toluca–Atlacomulco, Km 14.5, Unidad San Cayetano, 50200 Toluca, MEX, Mexico*

Correspondence should be addressed to R. Natividad; reynanr@gmail.com and A. Ramírez-Serrano; aramirezs@uaemex.mx

Received 7 May 2017; Revised 22 July 2017; Accepted 26 July 2017; Published 28 January 2018

Academic Editor: Detlef W. Bahnemann

This work focuses on modeling and simulating the absorption and scattering of radiation in a photocatalytic annular reactor. To achieve so, a model based on four fluxes (FFM) of radiation in cylindrical coordinates to describe the radiant field is assessed. This model allows calculating the local volumetric rate energy absorption (LVREA) profiles when the reaction space of the reactors is not a thin film. The obtained results were compared to radiation experimental data from other authors and with the results obtained by discrete ordinate method (DOM) carried out with the Heat Transfer Module of Comsol Multiphysics® 4.4. The FFM showed a good agreement with the results of Monte Carlo method (MC) and the six-flux model (SFM). Through this model, the LVREA is obtained, which is an important parameter to establish the reaction rate equation. In this study, the photocatalytic oxidation of benzyl alcohol to benzaldehyde was carried out, and the kinetic equation for this process was obtained. To perform the simulation, the commercial software COMSOL Multiphysics v. 4.4 was employed.

1. Introduction

In the last decades, photocatalytic processes have been the subject of different studies such as wastewater treatment [1–6], air purification in polluted environments with volatile organic compounds [7–9], and synthesis of fine organic compounds such as benzaldehyde [10, 11]. According to literature [1, 3–6, 11–16], the following different variables are crucial in a photocatalytical process efficiency: (a) catalyst type and concentration, (b) reagent type and concentration, (c) geometry and type of reactor, and (d) characteristics of the radiation inside the photoreactor. Because of the number of variables and the interaction among them, the modeling of this type of processes is expected to be rather useful not only for reactor design but also to achieve a better insight and understanding of the process.

The mathematical modeling and simulation of a photocatalytic reactor imply a great challenge due to the numerous involved variables; however, the computational analysis of these variables aids to accomplish such a task. Furthermore, the computational analysis allows evaluating hydrodynamic effects and kinetics without employing physical prototypes. The full modeling of photocatalytic reactors requires to include several submodels to simulate the physical phenomena occurring inside the reactor. Some of these necessary submodels are (a) radiation emission and incidence, (b) radiation absorption and scattering, (c) photoconversion kinetics, and (d) hydrodynamics [5, 13–15, 17, 18]. These are the result of mass, energy, and momentum balances, as well as radiation distribution and optical characterization of reaction space [6, 16, 19, 20]. These submodels are strongly interlinked. For example, the kinetics is a function of radiation absorption, which is in turn a function of catalyst characteristics and hydrodynamics. The conversion and performance of a photocatalytic reaction are a function of the local volumetric rate energy absorption (LVREA), which is

defined as the energy due to photons absorbed per time and volume inside the photoreactor [21]. To evaluate the LVREA is necessary to solve the radiation transfer equation (RTE) [22–25].

$$\frac{dI_\lambda(x,\Omega)}{dx} = -\beta_\lambda I_\lambda(x,\Omega) + \frac{\sigma_\lambda}{2}\int_{4\pi} I_\lambda(x,\Omega)p\left(\Omega \to \Omega^{'}\right)d\Omega, \tag{1}$$

where $I_\lambda(x,\Omega)$ is the spectral radiation intensity, λ represents the wavelength, β_λ is the extinction coefficient, which is the sum of the absorption coefficient, κ_λ, and σ_λ is the scattering coefficient. The ratio $\omega = \sigma_\lambda/\beta_\lambda$ is the scattering albedo coefficient which is inherent to each photocatalyst since it represents its photon absorption capacity. Ω is the solid angle, and $p(\Omega \to \Omega^{'})$ is the phase function representing the redistribution of radiation after the scattering event. According to the first term in the right side of (1), the intensity is diminished by the effect of mainly two phenomena, scattering and absorption. This decrease is characterized by the extinction coefficient. There is also an increase in the intensity due to the scattering from other directions, and it is represented by the second term in the right-hand side of (1) [24, 26, 27].

The analytical solution of the RTE is a rather complex task, unless it is limited to simple reactor geometries with specific assumptions. Even when using specialized software, the radiation field simulation is a task that requires a high computational effort. Comsol Multiphysics v. 4.4 contains the physics of radiation in participating media (rpm), in the Heat Transfer Module, which is designed to solve 3D radiation transfer problems, taking into account the phenomena of emission, dispersion, and absorption of radiation. The Comsol Multiphysics v. 4.4 Heat Transfer Module employs the discrete ordinate method (DOM). This method consists the transformation of the integral-differential RTE into a system of algebraic equations to describe the transport of photons in such way that can be solved following the direction of propagation, starting from the values provided by the boundary conditions. However, RTE is solved by discretizing the solid angle at every discrete position in the 3D domain, which is computationally very demanding and may result in unrealistic results when the discretization of the solid angle is not refined enough.

A viable alternative is to employ numerical computational methods as the statistical method Monte Carlo (MC), which is known as highly accurate but requires a great computational effort [21, 28, 29]. Also, it is possible to employ analytical simplified methods like the two-flux model (TFM) and the six-flux model (SFM). These models consist of several algebraic equations developed for flat slab geometries [15–17, 30], which were obtained by solving a system of differential equations with specific boundary conditions, for example, the outer wall of the reactor is opaque. SFM is very accurate for cylindrical geometries [14] in which the space where the reaction occurs, δ, is much smaller than the radius of the reactor, R_R.

$$\delta \ll R_R, \qquad \frac{R_R}{R_R + \delta} \sim 1. \tag{2}$$

However, in this investigation, a reactor in which the lamp is immersed in the reaction medium was used, so (2) is not satisfied. The geometry used in this work is shown in Figure 1. This paper aims to evaluate the effectiveness of a modified model based on four flux of radiation (FFM), whose equations are based on a cylindrical geometry, to mathematically represent the radiation field in a stirred annular photoreactor. This model is coupled to a reaction rate model representing the benzyl alcohol oxidation. The FFM evaluates the incident radiation in each point of the reaction space. This model considers that the incident radiation is the sum of radiation fluxes traveling from the light source towards this point and the fluxes due from both axial and radial scattering. As this model is developed from cylindrical geometries, its solution is expected to better represent the radiant field inside an annular photocatalytic reactor than the models developed from slab plane geometries where the reaction space is only a thin film.

The main objective of this work was to validate the proposed four-flux model, which is specifically designed for annular photocatalytic reactors with a relationship, that is, the reactor is not thin-walled. FFM is tested against the results with experimental data of the photocatalytic and selective oxidation of benzyl alcohol towards benzaldehyde. Moreover, the radiation profiles were compared to those calculated by MC, DOM, and SFM. The FFM and DOM were carried out with commercial software Comsol Multiphysics 4.4, which is a powerful differential equation solver.

2. Methodology

The main objective of this work was to test a proposed FFM to efficiently represent the radiant field inside an annular reactor when the reaction space is not a thin film. In order to validate the proposed model, the profiles obtained with FFM were compared to those previously reported in the literature. Also, the FFM was applied to describe the radiant field in a batch annular photoreactor employed to experimentally obtain benzyl alcohol oxidation data. Then, the kinetics of this reaction was established as function of LVREA.

2.1. Source Data

2.1.1. System 1. The profiles obtained in a thin-film slurry reactor of inner wall (TFSIW) reported by Li Puma et al. [5, 14, 17] and obtained by the six flow model were replicated for comparison purposes. In this case, the relation $R_R/(R_R + \delta) = 0.76$. The characteristics of the system are summarized in Table 1.

2.1.2. System 2. This photoreactor was previously reported [28, 29] and was named Photo-CREC Water II and employs TiO_2 (anatase) as a catalyst. In such a reaction system, the lamp is annulus centered. The relationship

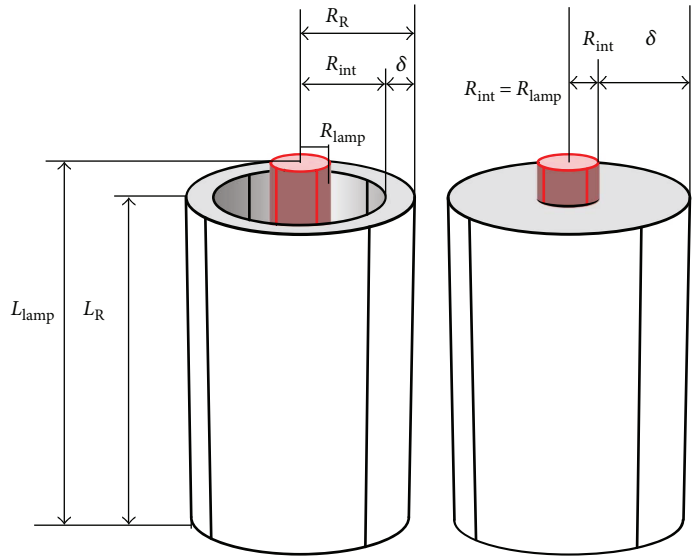

Figure 1: Schematic representation of the geometry of the assessed annular photocatalytic reactor.

Table 1: Characteristics of systems.

	Catalyst	Lamp characteristics	Reactor characteristics
System 1 Li Puma [14]	TiO_2 DP 25 (i) $\sigma_\lambda = 1.02\ C_{cat}$ (1/m) (ii) $\kappa_\lambda = 0.338\ C_{cat}$ (1/m)	Power: 4 W Wavelength: 300 nm Radius: 0.00775 m Length: 0.213 m	Length: 0.225 m Ext. radius: 0.019 m Int. radius: 0.013 m $R_R/(R_R + \delta) = 0.76$
System 2 Moreira et al. [28, 29]	TiO_2 anatase (i) $\sigma_\lambda = 3.1149\ C_{cat}$ (1/m) (ii) $\kappa_\lambda = 0.3957\ C_{cat}$ (1/m)	Power: 8 W Wavelength: 250 nm Radius: 0.0133 m Length: 0.413 m	Length: 0.445 m Ext. radius: 0.0444 m Int. radius: 0.01755 m $R_R/(R_R + \delta) = 0.62315$
System 3	$LiVMoO_6$ (i) $\sigma_\lambda = 0.24128\ C_{cat}$ (1/m) (ii) $\kappa_\lambda = 0.03092\ C_{cat}$ (1/m)	Power: 8 W Wavelength: 254 nm Radius: 0.005 m Length: 0.23 m	Length: 0.25 m Ext. radius: 0.025 m Int. radius: none $R_R/(R_R + \delta) = 0.5555$

$R_R/(R_R + \delta) = 0.62315$. The characteristics of the system are also summarized in Table 1.

2.1.3. System 3. Once the radiation model was validated with data reported in systems 1 and 2, this model was applied to simulate the radiation field in system 3 during benzyl alcohol selective oxidation towards benzaldehyde. Experimental data of benzyl alcohol oxidation were obtained in an annular cylindrical photocatalytic reactor. It is worth pointing out that in this reaction system, the lamp was placed at the center of the reactor without any additional physical protection (e.g., quartz sleeve). For this reason, the relationship $R_R/(R_R + \delta) = 0.5555$.

The employed catalyst was $LiVMoO_6$, and a detailed characterization has been previously reported [31]. The characteristics of the system are shown in Table 1. The FFM was used to describe the radiant field in this reactor and to obtain the kinetics of benzyl alcohol oxidation as a function of LVREA.

2.2. Mathematical Modeling of Radiation Emission. The emission of radiation from the cylindrical lamp is modeled using the linear source spherical emission (LSSE). This model considers that the lamp is a linear source, and each point on the line emits radiation isotropically and in every direction. It is assumed that the radiation emitted by each point of the lamp is constant along the axial length of the lamp [5]. According to the literature, the intensity of the incident radiation entering the inner wall of the annulus can be calculated as

$$I_{R_{int},Z} = \frac{S_1}{4\pi R_{int}} \left[a\tan\left(\frac{2z - L_R + L_{lamp}}{2R_{int}}\right) - a\tan\left(\frac{2z - L_R - L_{lamp}}{2R_{int}}\right)\right], \quad (3)$$

where

$$S_1 = 2\pi R_{lamp} I_w. \quad (4)$$

The experimental emitted radiation was measured by a UVX radiometer equipped with a sensor of 254 nm placed at the lamp wall and 0.01 m from the lamp.

2.3. Mathematical Modeling of Absorption and Scattering Radiation. To establish the mathematical FFM, the following assumptions were made: (a) reactor with slurry catalyst, (b) heterogeneous model, (c) isothermal process, (d) perfect mixing and therefore the catalyst concentration is homogeneous at all reaction space, (e) photons are absorbed only by catalyst particles, (f) the flux of photons occurs only in four directions, two radial, and two axial directions, (g) the emission of photons by the lamp is isocratic, (h) oxygen bubbles do not affect the radiation fluxes, and (i) the scattering of photons by the catalyst is isotropic.

FFM was employed to evaluate the incident radiation on a given point inside the reaction space. In this model, the total radiation flux is taken as the sum of the flux of photons traveling from the light source towards that point and flux of photons from scattering in both two axial directions and two both radial directions. In concordance, a photon balance was performed in a differential volume element shell shaped in cylindrical coordinates (Figure 2).

The flux of incident radiation (g_f), the flux entering the differential element due to backscattering (g_b), and the fluxes entering from bottom and upper walls (g_a and g_c) are the four fluxes that this model accounts for. The parameters p_f, p_b, p_a, and p_c represent the probabilities of occurring backscattering in the corresponding directions. These parameters were calculated by MC method employing an isotropic phase function, and their values are $p_f = 0.405, p_b = 0.303$, $p_a = 0.146$, and $p_c = 0.146$ for $LiVMoO_6$ and $p_f = 0.357, p_b = 0.351, p_a = 0.146$, and $p_c = 0.146$ for TiO_2. The number and external area of the catalytic particles are n_p and a_p, respectively, so in order to establish that the FFM is necessary to perform a balance of incident radiation (g_f), in the four considered directions. For example, the following radiation balance in the radial direction can be written as

$$\{\text{Input photons}\} - \{\text{output photons}\} = \{\text{absorbed photons}\}. \tag{5}$$

So the balance is

$$\begin{aligned} g_f(2\pi r\Delta z)|_r - g_f(2\pi r\Delta z)|_{r+\Delta r} + g_b\omega(2\pi r\Delta r\Delta z)\left(n_p a_p p_b\right) \\ + g_a\omega(2\pi r\Delta r\Delta z)\left(n_p a_p p_a\right) + g_c\omega(2\pi r\Delta r\Delta z) \\ \cdot \left(n_p a_p p_c\right) - g_f\left(n_p a_p(\omega p_a + \omega p_b + \omega p_c)\right) \\ \cdot (2\pi r\Delta r\Delta z) \\ = g_f(1-\omega)\left(n_p a_p\right)(2\pi r\Delta r\Delta z). \end{aligned} \tag{6}$$

By reordering and applying $\lim_{\Delta r\to 0}$,

$$\frac{d(rg_f)}{dr} = \left(\frac{r}{\beta\cdot C_{cat}}\right)(\omega(g_b p_b + g_a p_a + g_c p_c) - g_f(1-\omega p_f)), \tag{7}$$

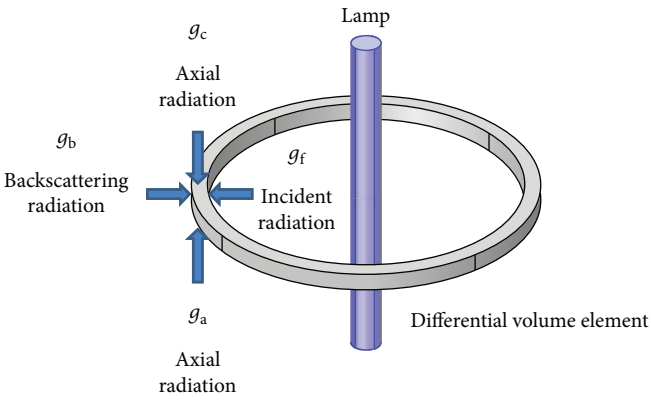

Figure 2: Directions of the fluxes of photons in the four-flux model.

where

$$\omega p_b + \omega p_a + \omega p_c + \omega p_f + (1-\omega) = 1, \tag{8}$$

$$\left(\frac{1}{(1/n_p a_p)}\right) = \left(\frac{1}{\beta C_{cat}}\right). \tag{9}$$

The term $(1/(1/n_p a_p))$ is the extinction characteristic length. It has been suggested [5] that the extinction characteristic length can be replaced by the inverse of the extinction volumetric coefficient $(1/\beta C_{cat})$. Physically, this represents the mean free path of the photons in the slurry. Doing a similar balance in the backscattering directions, the following equations are obtained:

$$\frac{d(rg_b)}{dr} = \left(\frac{r}{\beta\cdot C_{cat}}\right)(\omega(g_f p_b + g_a p_c = g_c p_a) - g_b(1-\omega p_f)), \tag{10}$$

$$\frac{d(rg_a)}{dz} = \left(\frac{r}{\beta C_{cat}}\right)(\omega(g_f p_c + g_b p_a + g_c p_b) - g_a(1-\omega p_f)), \tag{11}$$

$$\frac{d(rg_c)}{dz} = \left(\frac{r}{\beta\cdot C_{cat}}\right)(\omega(g_f p_a + g_a p_b + g_b p_c) - g_c(1-\omega p_f)). \tag{12}$$

Equations (7), (10), (11), and (12) are simultaneously solved by applying the following boundary conditions.

(1) BC 1: at wall lamp or inner wall:

$$\begin{aligned} g_f\left(r = R_{lamp}\right) &= I_{r,z}A_{lamp}p_f \\ g_b\left(r = R_{lamp}\right) &= (g_f + g_a + g_c)p_b \\ g_a\left(r = R_{lamp}\right) &= (g_f + g_b + g_c)p_a \\ g_c\left(r = R_{lamp}\right) &= (g_f + g_a + g_b)p_c. \end{aligned} \tag{13a}$$

(2) BC 2: at external reactor wall (opaque wall):

$$\begin{aligned} g_f(r = R_R) &= (I_{r,z} p_f)\exp(-\beta\delta) \\ g_b(r = R_R) &= 0 \\ g_a(r = R_R) &= (g_f + g_b + g_c)p_a \\ g_c(r = R_{lamp}) &= (g_f + g_a + g_b)p_c. \end{aligned} \tag{13b}$$

(3) BC 3: at upper and bottom wall:

$$g_a(z = L_R) = g_c(z = 0) = 0. \tag{13c}$$

These boundary conditions are shown in Figure 3. Furthermore, considering an infinitely long reactor, the following condition can be established, along the axial axis:

$$\frac{\partial g_a}{\partial z} = \frac{\partial g_c}{\partial z} = 0. \tag{14}$$

The LVREA using the four-flux model can be calculated by the following expression:

$$\text{LVREA} = \frac{g_{total}\kappa_\lambda}{V}\left(\frac{R_{lamp}\delta}{4r^2}\right). \tag{15}$$

2.4. Simulation of Radiant Field. The software COMSOL Multiphysics version 4.4 and subroutines performed in Matlab® were employed to solve the FFM and kinetic models, respectively. To carry out the simulation, the geometric domain of both, reaction space and lamp, was established. The model is two-dimensional and symmetric with respect to the axial axis. A nonuniform mesh was used, with a size of element calibrated to plasma, giving major emphasis on the inner wall of the annulus, using a fine mesh at this boundary and coarser in the outer wall of the reactor to accurately assess each border (Figure 4(a)). As a result, color maps are obtained, which represent the distribution of LVREA within the photocatalytic reactor. The red zone represents the highest values, and the colors are decreasing towards blue which represents low values of LVREA. The modeling instructions for FFM can be found in the complementary content (Appendix A).

The results obtained by FFM were compared with the following.

(A) Discrete ordinate method (DOM) carried out with the physics of radiation in participating media of the Heat Transfer Module of Comsol Multiphysics 4.4. To do so, the geometric domain of reaction space was established as 3D model. Several preliminary simulations were run using this method. In these trials, the mesh in all domains was refined incrementally until the physical ram limit of the workstation (8 Gb) was reached. Geometry and mesh employed are shown in Figure 4(b). The modeling instructions for DOM can be found in the complementary content (Appendix B).

(B) Six-flux model (SFM) was implemented in programming language Matlab according to the methodology reported by Li Puma [14, 17].

(C) Monte Carlo Method (MC) was also implemented in programming language Matlab based on Moreira et al. [28, 29]. In this case, the number of used photons was 1×10^7. In addition, subroutines were programmed to generate random numbers.

The codes to solve the applied models, SFM and MC, are rather lengthy. However, they can be provided upon request.

2.5. Kinetic Model. To determine the radiation effect on reaction rate, a kinetic expression as function of LVREA can be obtained.

$$\frac{dC_{AB}}{dt} = k_r f(C_{AB}) g(\text{LVREA}), \tag{16}$$

where $f(C_{AB})$ is a function of reagent concentration (benzyl alcohol) and the dependence of reaction rate with LVREA is given by $g(\text{LVREA})$. To describe $f(C_{AB})$ is possible to employ a power law model. This is accepted when the reagent absorption on the catalytic surface is negligible and therefore the LHHW model becomes a pseudo first-order equation. Although this kind of equation does not include the effect of reactive intermediaries, it still provides reasonable results [6, 11]. Several authors have studied the kinetics of photocatalytic oxidation of aromatic alcohols to corresponding aldehydes, and they claim a first-order kinetics regarding alcohol concentration [10, 11].

$$-\frac{dC_{AB}}{dt} = K_{Ap} C_{AB}, \tag{17}$$

where K_{Ap} is the apparent kinetic coefficient that includes the effect of catalyst concentration, temperature, oxidant concentration, and so forth. Furthermore, since there is reaction due to photolysis only (without catalyst), this can be considered within the reaction rate expression.

$$\left(\frac{-dC_{AB}}{dt}\right)_{Total} = \left(\frac{-dC_{AB}}{dt}\right)_{Without\ catalyst} + \left(\frac{-dC_{AB}}{dt}\right)_{With\ catalyst}, \tag{18}$$

$$\left(\frac{-dC_{AB}}{dt}\right)_{Total} = k_{r1} C_{AB} + k_{r2} C_{AB} = (k_{r1} + k_{r2}) C_{AB} = K_{Ap} C_{AB}, \tag{19}$$

where k_{r1} is the intrinsic constant of reaction rate without catalyst and k_{r2} is the reaction rate constant with catalyst, which is a function of LVREA. Therefore, K_{Ap} can be expressed as

$$K_{Ap} = k_{r1} + k_{r2} = k_{r3}(\text{LVREA})^m, \tag{20}$$

by linear regression, both the order of LVREA and k_{r3} were calculated. Employing the FFM method, the values of averaged LVREA corresponding to each catalyst concentration were calculated. The contribution due to photolysis is negligible; for this reason, the LVREA due to the reactive species was not added in the photolysis term. It is worth noticing that in other cases, when the reactant molecule has a strong absorption of photons, this contribution must also be taken into account. This also applies for intermediaries. In the present case, however, the reaction kinetics was established with

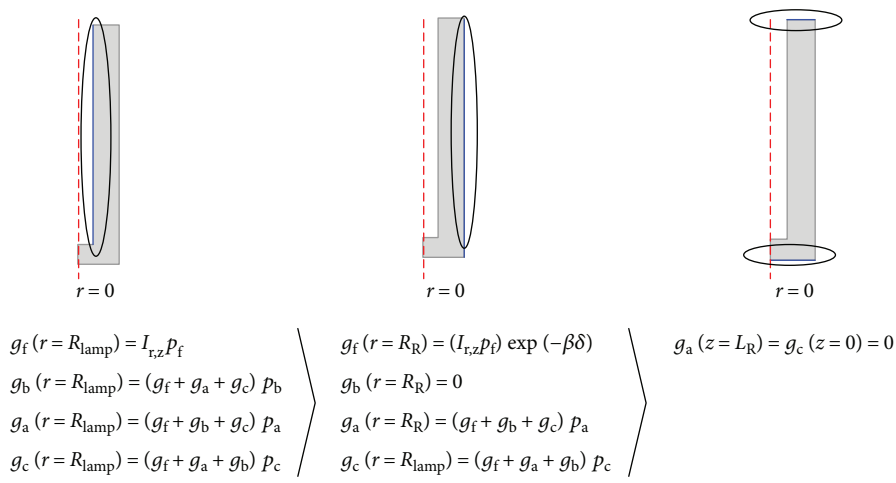

Figure 3: Boundary conditions used in the four-flux model.

very low conversion data and therefore the presence of intermediaries was considered rather low as to contribute to LVREA.

3. Results

3.1. Emission Model. Figure 5 shows the emitted radiation profiles calculated by both, MC and LSSE methods. In addition, the radiation values experimentally measured by a UVx radiometer equipped with a detector 254 nm were plotted. Figure 5(a) shows the values of the emitted radiation, $I_{(R_{lamp},z)}$ on the wall of the lamp, and Figure 5(b) shows the values of $I_{(R_{lamp}+0.01m,z)}$ at 0.01 m from the wall of the lamp. It can be seen that both methods are in good agreement with experimentally obtained data, which justifies the use of both Monte Carlo method and LSSE model in this research.

3.2. Absorption of Radiation Model. The results of the proposed model ((7), (8), (9), (10), (11), (12), (13a), (13b), (13c), (14), and (15)) were compared with those obtained by MC, SFM, and DOM. It was assumed that MC is the method that best represents the radiant field in the photocatalytic reactor. Even though the DOM is robust, it requires a very refined mesh to give congruent results.

3.2.1. System 1: TFSIW. The first analyzed photocatalytic reactor was a TFSIW reported by Li Puma et al. [5, 14, 17]. This reactor has a radius ratio $R_R/(R_R + \delta) = 0.76$. Figure 6 shows the radial profiles of LVREA at $z = L_R/2$ for this system, calculated by the four methods and parity diagram. It can be seen that SFM and DOM represent LVREA profiles better than the FFM with regard MC, especially when the catalyst concentration is low. However, FFM results can be considered to be adequate also if a rapid estimation of LVREA is required. Both the FFM and the SFM have small deviations in the inner wall when the catalyst loading is large. With the mesh used for the DOM, the computing time was approximately 40 minutes. Using a finer mesh could increase the computing time by several hours. The solving time for FFM was about 2 minutes regardless the elements number in the mesh.

3.2.2. System 2 (Photo-CREC II). The results obtained by FFM method are in agreement with the data previously reported by Moreira et al., which were obtained from MC for Photo-CREC water II [28, 29]. Figure 7 shows the radial profiles for the LVREA at different photocatalyst concentrations for TiO_2 anatase and parity diagram obtained by SFM, DOM, and FFM versus MC. In this case, it is observed that the results obtained by FFM and DOM are quite congruent although they tend to deviate slightly from those obtained by MC. This reactor has a ratio of radius $R_R/(R_R + \delta) = 0.6231$. The mesh used in DOM for this relationship can be considered as semicoarse and give good results in about 1 hour of computing time.

3.2.3. System 3. This system was theoretically and experimentally studied. Figure 8 shows the comparison of the LVREA profiles obtained from the three methods for the catalyst $LiVMoO_6$. It is worth noticing that the catalyst with the highest extinction coefficient values ($\beta = \sigma + \kappa$) (TiO_2 DP 25) produces higher values of LVREA at the same catalyst concentration. The values of LVREA obtained by $LiVMoO_6$ catalyst are smaller than the values obtained by TiO_2 catalyst; however, the special interest on $LiVMoO_6$ catalyst resides on that it presents catalytic activity even in the visible spectrum [31].

In Figure 8, it can be observed that near the lamp wall (dimensionless radius = 0.4), LVREA is maximum and rapidly decreases as dimensionless radius increases. This effect is considered by both, MC and FFM; however, the SFM does not account for it. This can be attributed to SFM being explicitly developed for thin-walled annular reactors and presents significant deviations when $R_R/(R_R + \delta) \ll 1$. Also, DOM presents a great deviation with respect to MC. This is because the meshing is not fine enough. However, using a more refined mesh causes the available RAM to be exceeded.

Table 2 shows a comparison of correlation coefficients for SFM, FFM, and DOM considering that MC is the most

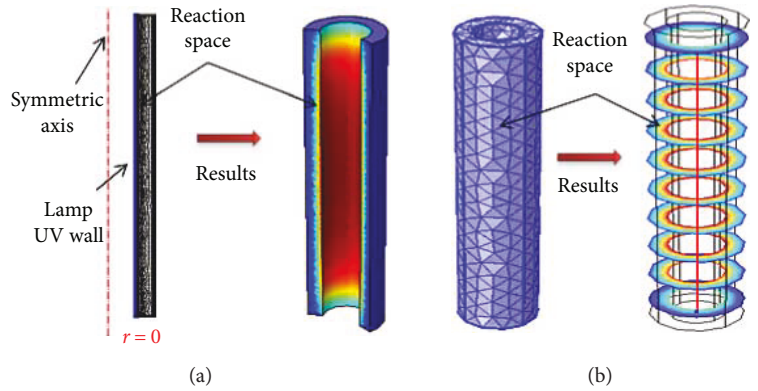

Figure 4: Graphical representation of photocatalytic reactor and geometry employed to solve (a) four-flux model and (b) discrete ordinate method, in COMSOL Multiphysics.

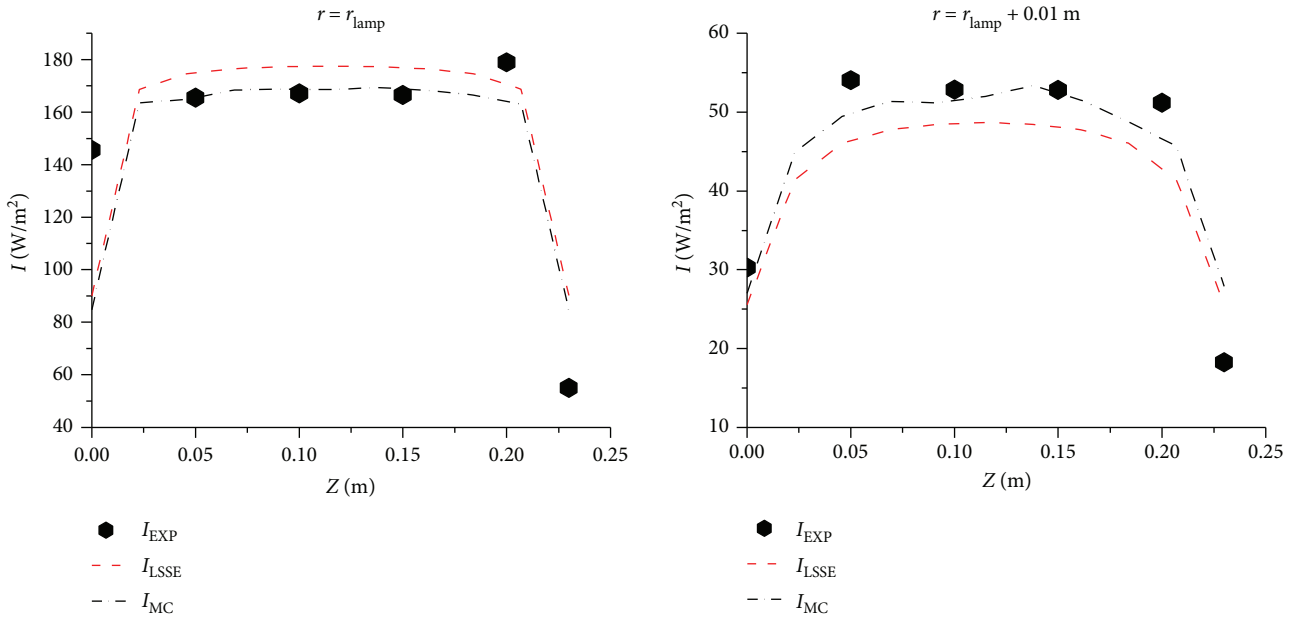

Figure 5: Emission model results. Calculated and experimental incident radiation profiles.

accurate one. The percentage of the area under the curve of the radiation profiles obtained by the different methods in relation to the area under the Monte Carlo method curve is also shown. It can be seen that the FFM better predicts the profiles of LVREA when $R_R/(R_R + \delta) \ll 1$ and the catalyst loading is relatively low, for example in system 3.

Through Figures 6, 7, and 8, it can be seen that near the inner wall of the reaction space, LVREA is maximum and rapidly decreases as dimensionless radius increases. This can be ascribed to an obstruction effect produced by catalyst particles. One can also notice that in cases where the photocatalyst concentration is relatively high, the particles closer to the inner radius absorb most of the radiation entering the reactor. According to the results, it may be seen that low values of LVREA are obtained at low catalyst concentrations; however, the effectively irradiated zone is greater. At high catalyst concentrations, high values of LVREA are achieved near the wall of the lamp; however, the effectively irradiated zone is drastically diminished in the radial direction. It is important to note this effect since it is desirable to obtain high values of LVREA, but at the same time maximize the irradiated zone. In dark zones, absorption of photons does not occur, which provokes the effective volume of the reaction being smaller, that is, the reactor volume is being subutilized. This effect is shown in Figure 9. A sufficiently high photocatalyst concentration produces zones with dark areas towards the external radius. Therefore, there is an optimal catalyst concentration that provides an optimal irradiated reactor space. Photocatalyst concentrations above this maximum show an essentially negligible effect on LVREA. This optimal concentration can be seen in Figure 10, and it is in agreement with those reported [28, 29] for TiO_2 catalyst (system 1 and system 2). For system 3, the optimal concentration is achieved at 1 kg/m^3.

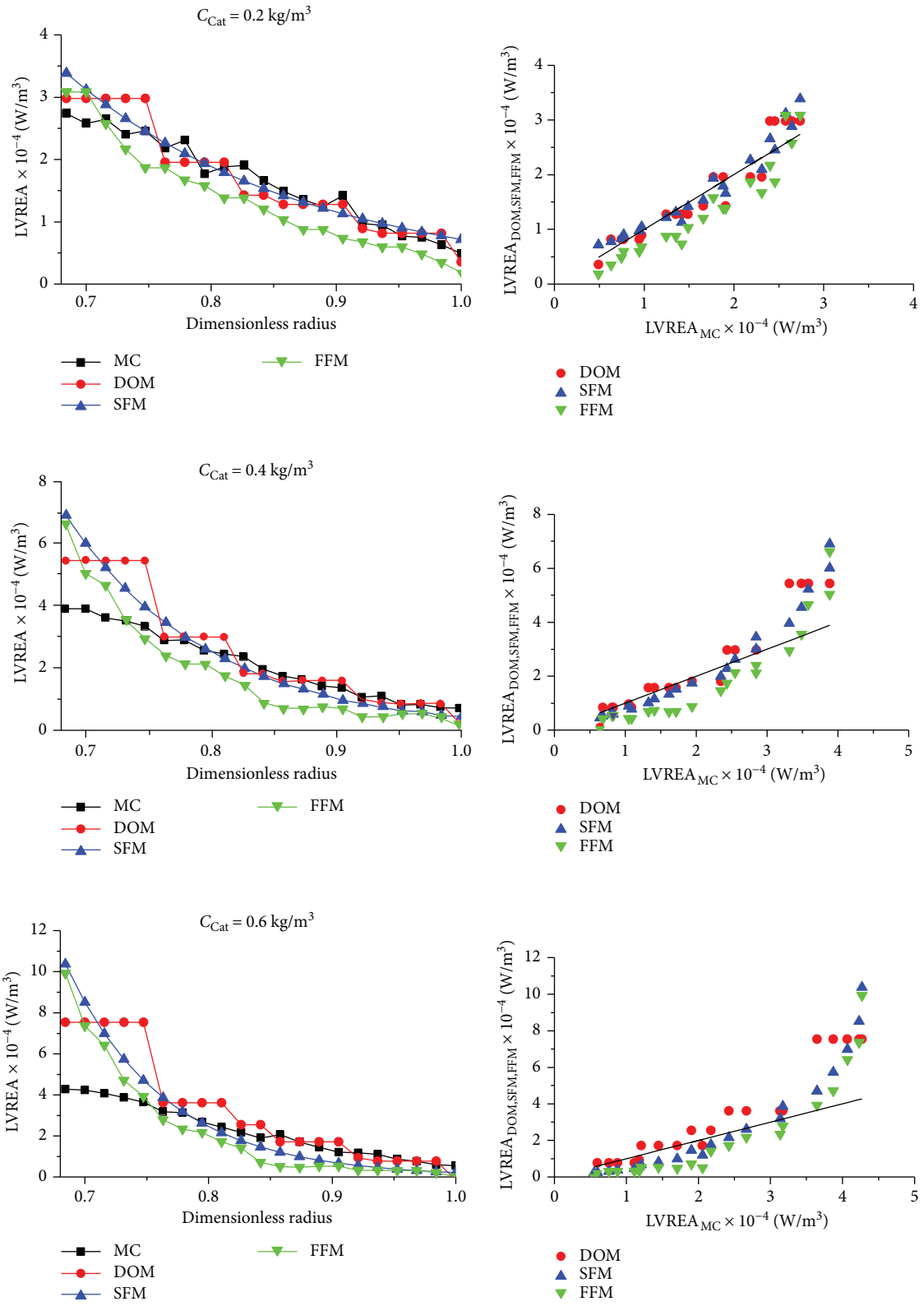

Figure 6: Radial profiles of local volumetric rate energy absorption (LVREA) obtained with four-flux model at different concentrations of catalyst for system 1 and its comparison with the other models.

3.3. Kinetic Model. To obtain a kinetic expression for photocatalytic oxidation of benzyl alcohol, the integral method was employed. An adjust by least squares was performed for different models, including the LHHW model, and it was found that the better adjustment is at pseudo first order in respect of concentration of benzyl alcohol. This

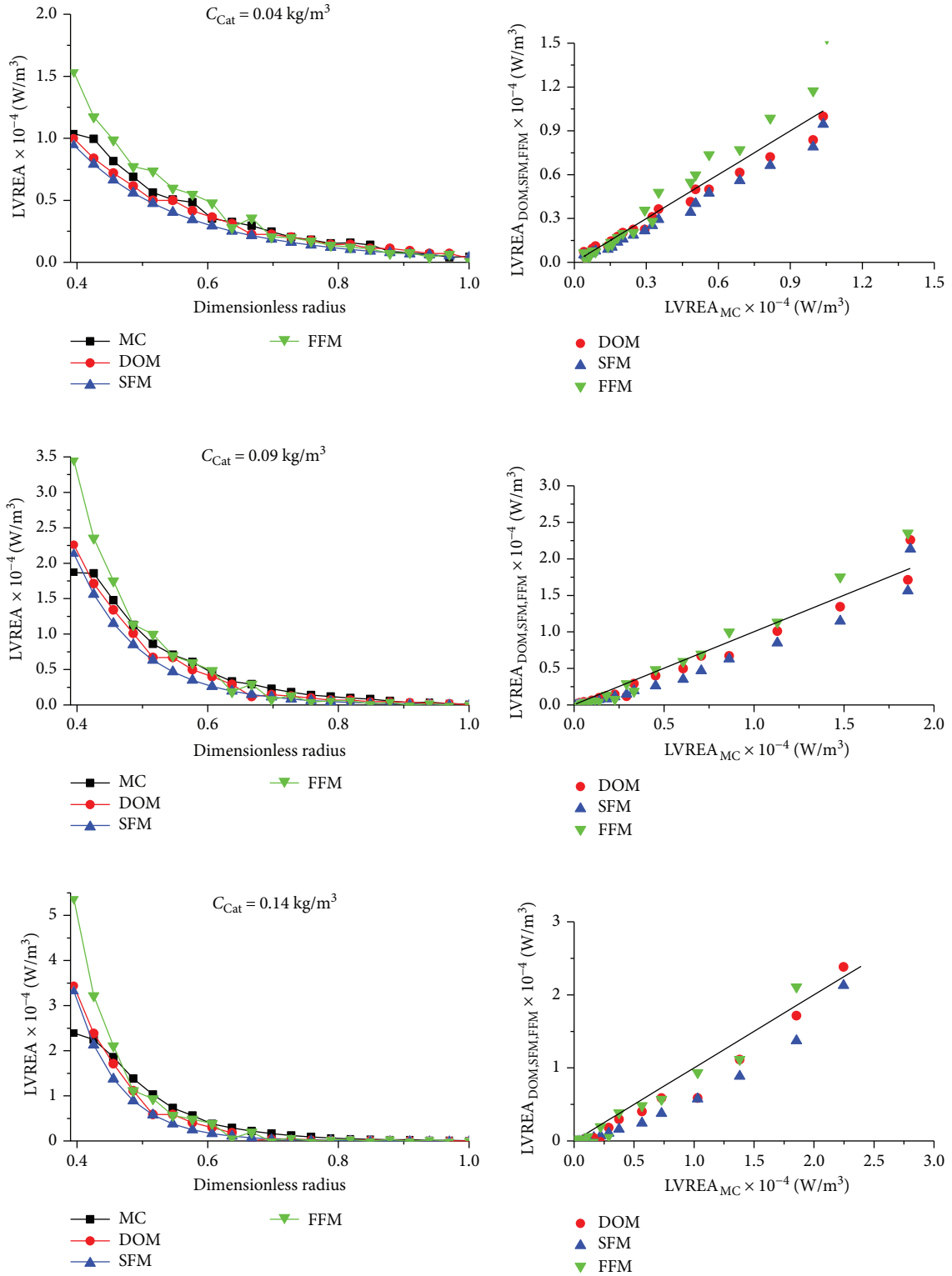

FIGURE 7: Radial profiles of local volumetric rate energy absorption (LVREA) obtained with four-flux model at different catalyst concentration for system 2 and its comparison with the other models.

result is in agreement with the results reported by [10, 11], albeit with other catalysts. Figure 11 shows the comparison of the results for the adjustment by least squares according to experimental data of benzyl alcohol oxidation, at different catalyst loading, employing a pseudo first-order power model.

Taking into account the data of concentration—time obtained at each catalyst loading, an adjustment by least

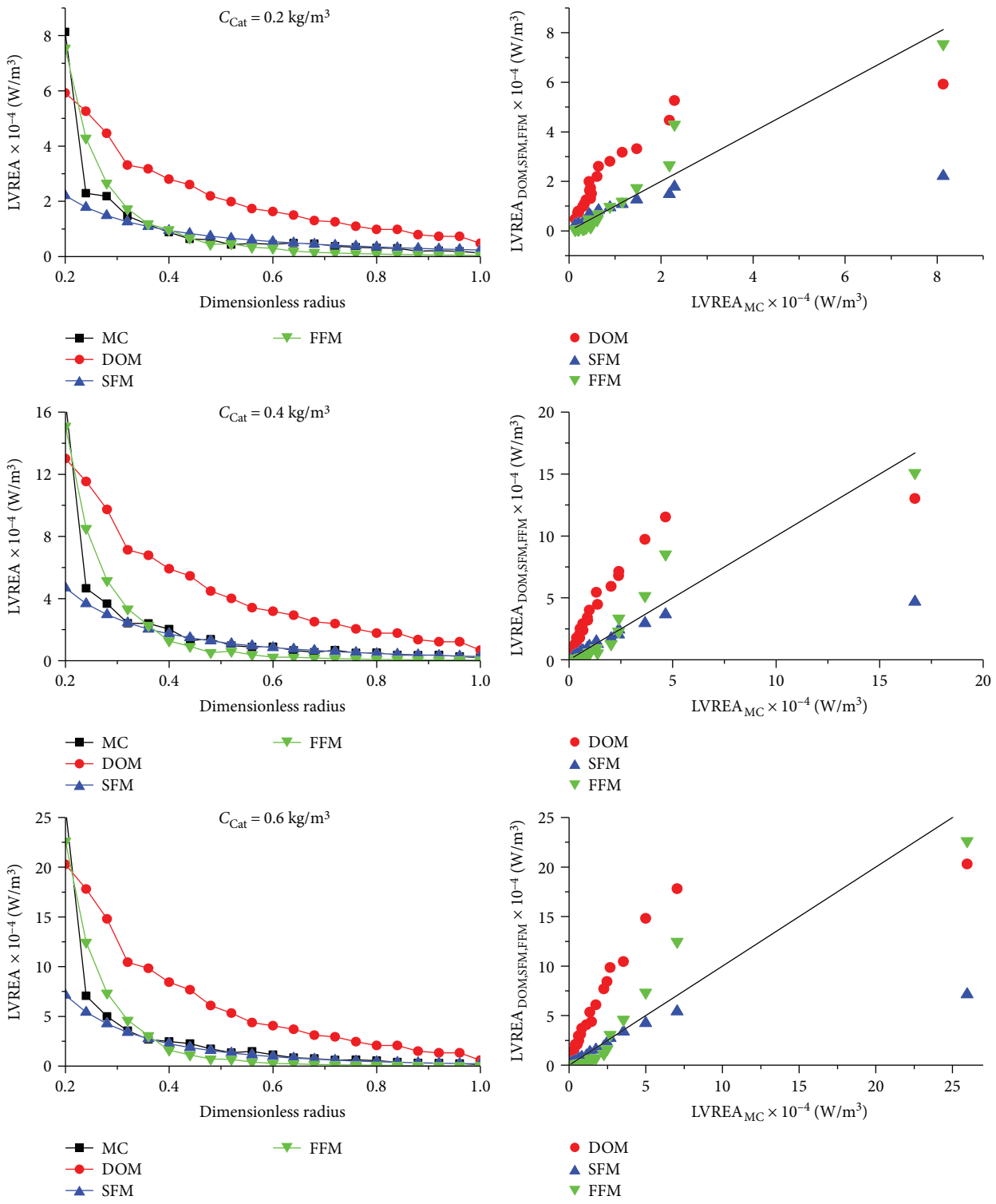

FIGURE 8: Radial profiles of local volumetric rate energy absorption (LVREA) obtained by four-flux model at different concentration of catalyst ($LiVMoO_6$) for system 2 and its comparison with the other models.

squares was performed to obtain the dependence of rate constants with the LVREA (Table 3).

Figure 12 shows the plot of $\ln(K_{Ap} - k_{r1})$ as a function of ln(LVREA). The slope of the line represents the order of the reaction with respect to the LVREA, and the intercept provides the $\ln(k_{r3})$. Hence $k_{r1} = 0.0101\ h^{-1}$, intrinsic reaction constant without catalyst; $k_{r3} = 0.01887\ h^{-1}(W/m^3)^{-0.1464}$; and $m = 0.1467$ is the power of LVREA. This fractional exponent of LVREA was expected. It has even been reported that the exponent is equal to 0.5 in the presence of TiO_2 for system 1 [18]. It

Table 2: Comparison of correlation coefficients of different radiation absorption models for studied systems.

System	Catalyst	C_{CAT} (mg/L)	DOM		SFM		FFM	
			R^2	$\%A_{MC}$	R^2	$\%A_{MC}$	R^2	$\%A_{MC}$
1 $R_R/(R_R+\delta)=0.76$	TiO_2	0.20	0.9530	101.69	0.9611	103.21	0.9458	80.78
		0.40	0.9602	120.54	0.9583	110.80	0.9167	84.22
		0.60	0.9595	143.91	0.9242	116.33	0.8906	94.20
2 $R_R/(R_R+\delta)=0.62315$	TiO_2 anatase	0.04	0.9943	91.83	0.9945	80.09	0.9868	114.16
		0.09	0.9833	88.33	0.9744	73.70	0.9642	110.29
		0.14	0.9629	87.47	0.9421	73.52	0.9285	113.02
3 $R_R/(R_R+\delta)=0.5555$	$LiVMoO_6$	0.20	0.8089	237.11	0.8468	81.79	0.9605	100.88
		0.40	0.8004	257.06	0.8518	76.16	0.9553	95.18
		0.60	0.7984	258.14	0.8571	70.79	0.9564	95.73

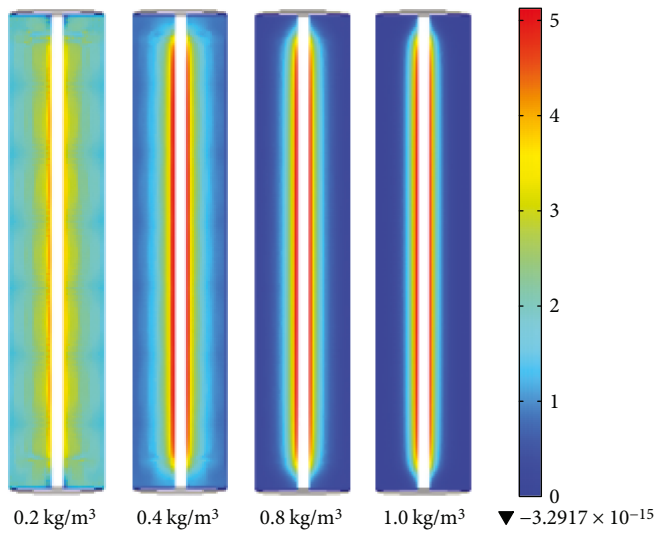

Figure 9: Effect of catalyst concentration on the reactor radial section where photon absorption occurs (LVREA map) in system 3.

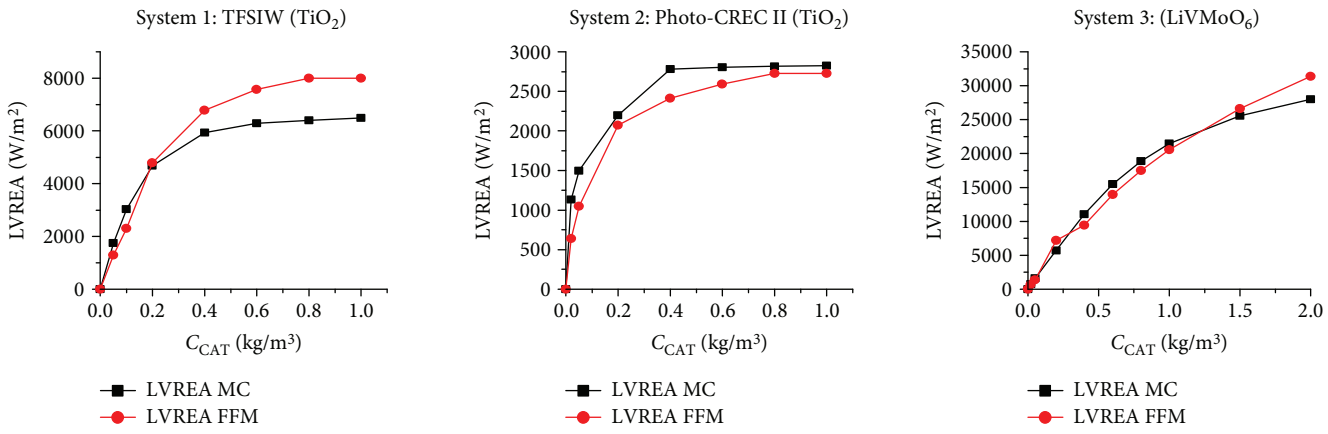

Figure 10: Simulated results of incident radiation as function catalyst loading.

should be noted that the value of m is relatively independent on the type of substrate. Instead, it should be dependent on the radiation intensity level over the catalyst. A fractional order dependence of photocatalytic reaction rate from the LVRPA is obtained when the rate of electron-hole recombination in the catalyst particles becomes predominant [18].

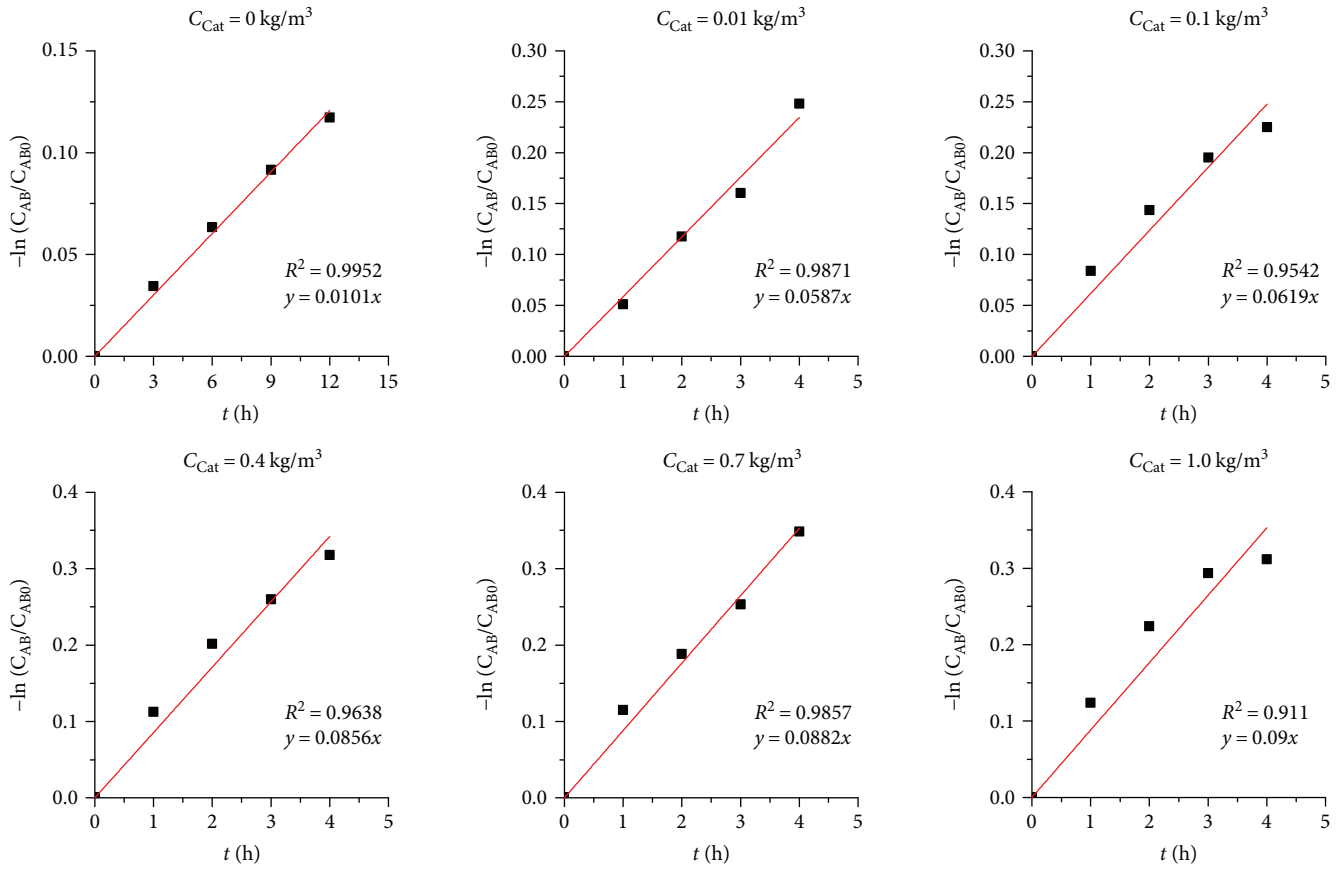

Figure 11: Test for a pseudo first-order kinetics as a function of concentration.

Table 3: First-order kinetic constants and values of LVREA at different catalyst loadings.

C_{cat} (kg/m^3)	K_{Ap} (h^{-1})	LVREA (W/m^3)
0.00	0.0101	0.00
0.01	0.0587	630.00
0.10	0.0750	5300.00
0.40	0.0856	13600.00
0.70	0.0882	16700.00
1.00	0.0900	18000.00

Therefore, the kinetic equation that describes the photocatalytic oxidation of benzyl alcohol to benzaldehyde is

$$-\frac{dC_{AB}}{dt} = \left(0.0101\,\mathrm{h}^{-1} + 0.01887\,\mathrm{h}^{-1}\left(\frac{\mathrm{W}}{\mathrm{m}^3}\right)^{-0.1464}(\mathrm{LVREA})^{0.1464}\right)C_{AB}. \quad (21)$$

Equation (20) shows that the reaction rate depends on the LVREA values and the amount of irradiated catalyst. Figure 13 shows the concordance of the proposed mathematical model with experimental data of benzyl alcohol oxidation at different catalyst loadings.

In Figure 13, a linear decrease of benzyl alcohol concentration is observed. This is in agreement with that previously reported [10, 11]. On the other hand, the conversion increases with the catalyst loading up to a point where a further increase on catalyst loading does not produce a significant improvement on conversion, due to LVREA reaches a maximum at this point, establishing that the optimal catalyst loading is 1.0 kg/m^3 for $LiVMoO_6$.

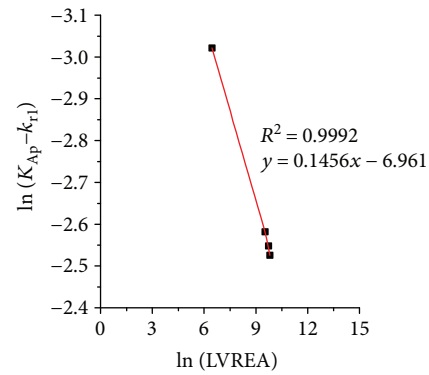

Figure 12: Adjustment for dependence of K_{Ap} with the LVREA.

4. Conclusions

The proposed mathematical model (FFM) describes the radiant field in a photocatalytic annular reactor. Its

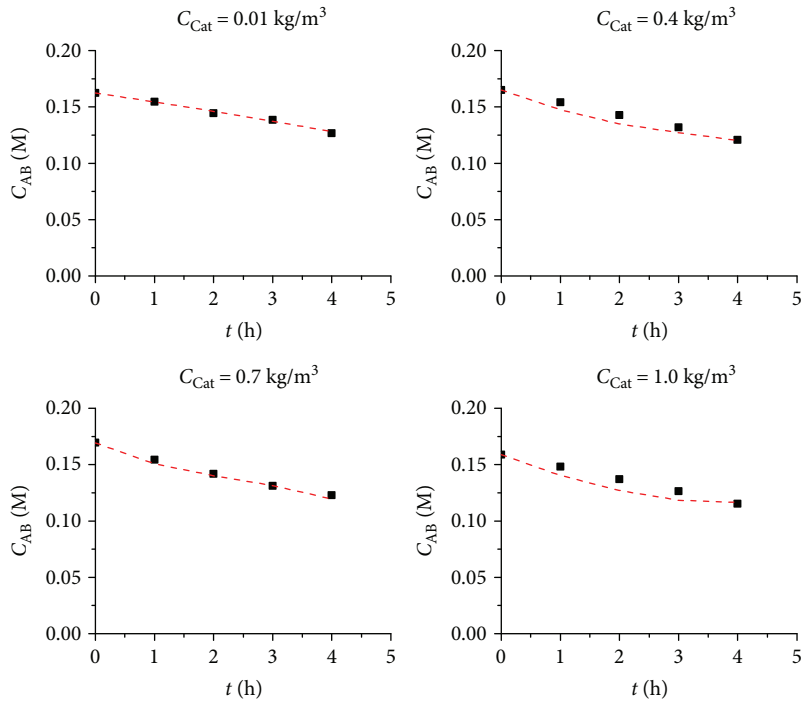

Figure 13: Comparison of experimental concentration profiles (dots) with those obtained by the proposed model.

numerical solution corresponds appropriately with experimental and numerical data, and it requires a minor computational effort than the other models, such as DOM, which is very robust and accurate but requires a high RAM capacity. The FFM was specifically designed for cylindrical geometries with the lamp located at the axial axis of the reactor submerged in reaction medium. The FFM predicts the LVREA profiles better than the other models when $R_R/(R_R + \delta) \ll 1$, and the catalyst loading is low.

The obtained kinetic equation describes the reaction rate in the photocatalytic reactor for selective oxidation of benzyl alcohol as function of the LVREA. The FFM allows the evaluation of LVREA at different catalyst loadings, power lamp, or reactor dimensions. Therefore, it allows the calculation of reaction rates at different experimental setups.

Within the range of studied variables, the reaction rate of the selective oxidation of benzyl alcohol adequately fits a first-order kinetics, where the kinetic coefficient is a function of LVREA, and this depends on catalyst loading, power lamp, and annulus width.

Appendix

A. Simulation of Radiant Field Employing the Four-Flux Model (FFM) in Comsol Multiphysics v. 4.4

(1) Model 2D: from the File menu, choose New. In the New window, click Model Wizard and select a 2D axisymmetric model.

(2) Interface for ordinary differential equations, ODE: in the Select Physics tree, select Mathematics > ODEs Interface > ODEs in general form (g). Click Add. The Study is Stationary.

(3) Parameters: go to Global definitions section and insert Parameters. In the Settings window for Parameters, locate the Parameters section and add the necessary parameters, such as reactor dimensions (reactor length, internal radius, and external radius), dispersion probabilities (p_f, p_b, p_a, and p_c), characteristics of the lamp (power, dimensions, and wavelength), catalyst charge, and optical properties of catalyst (absorption, kappa_s; dispersion, sigma_s; and extinction coefficients, beta_s), from Table 1.

(4) Global variable: go to Global definitions section and insert Variables. In the Settings windows for Variable, write the expression for radiation intensity (Irz), according to (3) and (4).

(5) Geometry: set reactor geometry as rectangular section that represents the 2D axial section of the reactor. It can be drawn as a simple rectangle.

(6) Model definitions: in model definitions, insert section for variables. In the Settings windows for Variable, insert the LVREA expression. It can be introduced with (15).

(7) Set of differential equations: in the ODE interfaces, select all domains. Go to the ODE general form window settings and introduce the differential equations system defined for (7), (10), (11), and (12).

(8) Incident intensity boundary: in ODE interfaces, insert a Dirichlet boundary condition. In this setting section, select the internal boundary (inner radius of reaction section). Locate boundary condition field and introduce (13a).

(9) External wall boundary condition: in ODE interfaces, insert a Dirichlet boundary condition. In this setting section, select the external boundary (external radius of reaction section). Locate boundary condition field and introduce (13b).

(10) Upper and bottom wall boundary condition: in ODE interfaces, insert a Dirichlet boundary condition. In this setting section, select the upper and bottom boundary. Locate boundary condition field and introduce (13c).

(11) Weak form of ODE: in ODE interfaces, insert a Weak Form for ODE condition. In this setting section, select all domains. In Weak expression field, introduce the following expressions:

WEAK = 0; 0; −test(gaz)*gaz + test(ga); −test(gcz)*gcz + test(gc).

(12) Mesh: in the mesh section, introduce a mesh using the option of free quadratic mesh. You can try different mesh sizes. In free quadratic mesh, add distribution, select inner wall and locate the input section, and introduce 500 in number of elements.

(13) Go to the study section and Run model.

B. Simulation of Radiant Field Employing the Discrete Ordinate Method (DOM) in Comsol Multiphysics v. 4.4

(1) Model 3D: from the File menu, choose New. In the New window, click Model Wizard and select a 3D model.

(2) Radiation in participating media: in the Select Physics tree, select Heat Transfer > Radiation > Radiation in Participating Media (rpm). Click Add. The Study is Stationary.

(3) Parameters: go to Global definitions section and insert Parameters. In the Settings window for Parameters, locate the Parameters section and add the necessary parameters, such as reactor dimensions (reactor length, internal radius, and external radius), characteristics of the lamp (power, dimensions, and wavelength), catalyst charge, and optical properties of catalyst (absorption, kappa_s; dispersion, sigma_s; and extinction coefficients, beta_s)

(4) Global variable: go to Global definitions section and insert variables. In the Settings windows for Variable, write the expression for radiation intensity (Irz), according to (3) and (4).

(5) Geometry: set reactor geometry as annular section. It can be drawn as a Boolean difference from two cylinders.

(6) Model definitions: in model definitions, insert section for variables. In the Setting windows for Variable, insert the LVREA expression. It can be introduced as LVREA = rpm.G*kappa.

(7) Radiation in participating media (rpm): in the physics for radiation in participating media go to Radiation with participating media window settings and introduce dispersion and absorption coefficients in the model input sections.

(8) In radiation in participating media, insert Incident intensity section. In this setting section, select the internal boundaries. Locate the incident intensity field and introduce Irz variable.

(9) Opaque surface: in radiation in participating media, insert opaque surface. In the setting section, select external boundaries of contours of the domain. In wall adjust, select Black Wall.

(10) Mesh: in the mesh section, introduce a mesh using the option of free tetrahedral mesh. You can try different mesh sizes. A too fine mesh can cause the available RAM to be exceeded.

(11) Go to the study section and Run model.

Nomenclature

a_{lamp}: Area of lamp (m^2)
a_p: Catalytic particle area (m^2)
C_{AB}: Benzylic acid concentration ($mol \cdot dm^{-3}$)
C_{cat}: Catalyst concentration ($kg \cdot m^{-3}$)
g_f: Flux incident radiation ($Watts \cdot m^{-2}$)
g_a: Upwards flux scattering radiation ($Watts \cdot m^{-2}$)
g_b: Flux backscattering radiation ($Watts \cdot m^{-2}$)
g_c: Downwards flux scattering radiation ($Watts \cdot m^{-2}$)
I_λ: Spectral radiation intensity ($Watts \cdot m^{-2} \cdot sr^{-1}$)
K_{Ap}: Apparent reaction constant (s^{-1})
k_{r1}: Intrinsic reaction constant without catalyst (s^{-1})
k_{r2}: Reaction constant with catalyst (s^{-1})
k_{r3}: Intrinsic reaction constant with catalyst ($Watts^{(-m)} \cdot m^{(3m)}$)
L: Length (m)
L_{lamp}: Length of lamp (m)
L_{Reac}: Length of the reactor (m)
LVREA: Local volumetric rate of absorption of energy ($Watts \cdot m^{-3}$)
m: Reaction order with respect to LVREA
n_p: Number of catalyst particles (m^{-3})
p_a: Probabilities of scattering toward up
p_b: Probabilities of backscattering
p_f: Probabilities of forward scattering
$p(\Omega \to \Omega')$: Phase function

r: Radial coordinate (m)
R_{int}: Inner radius of the annulus (m)
R_{lamp}: Radius of lamp (m)
R_R: Radius of reactor (m)
t: Time (h)
V: Volume (m^3)
X: Conversion
z: Coordinate axial (m).

Greek Letters

β_λ: Extinction coefficient (m^{-1})
Δ: Thickness of the annulus (m)
κ_λ: Absorption coefficient (m^{-1})
λ: Wavelength
σ_λ: Scattering coefficient (m^{-1})
ω: Albedo coefficient
Ω: Solid angle (sr).

Acronyms

DOM: Discrete ordinate method
FFM: Four-flux model
LVREA: Local volumetric rate of energy absorption
LHHW: Langmuir–Hinselwwod–Hougen–Watson kinetic model
MC: Monte Carlo model
RTE: Radiation transfer equation
SFM: Six-flux model
TFM: Two-flux model
TFSIW: Thin-film slurry reactor of inner wall.

Conflicts of Interest

The authors declare that they have no conflicts of interest.

Acknowledgments

The authors are grateful to PRODEP for the financial support through Project 103.5/13/5257 and CONACYT through Project 269093. Mr. O. Alvarado-Rolon is grateful to CONACYT for the financial support (Scholarship 401273) to conduct postgraduate studies. Citlalit Martínez Soto is acknowledged for the technical support.

References

[1] H. I. De Lasa, B. Serrano, and M. Salaices, *Photocatalytic Reaction Engineering*, Springer, 2005, April 2016 http://link.springer.com/content/pdf/10.1007/0-387-27591-6.pdf.

[2] L. F. Garcés Giraldo, E. A. Mejía Franco, and J. J. Santamaría Arango, "La fotocatálisis como alternativa para el tratamiento de aguas residuales," *Revista Lasallista de investigación*, vol. 1, pp. 83–92, 2004.

[3] G. Li Puma and P. L. Yue, "A novel fountain photocatalytic reactor for water treatment and purification: modeling and design," *Industrial and Engineering Chemistry Research*, vol. 40, no. 23, pp. 5162–5169, 2001.

[4] L. Zhang, W. Anderson, and Z. Zhang, "Development and modeling of a rotating disc photocatalytic reactor for wastewater treatment," *Chemical Engineering Journal*, vol. 121, no. 2-3, pp. 125–134, 2006.

[5] G. Li Puma, J. N. Khor, and A. Brucato, "Modeling of an annular photocatalytic reactor for water purification: oxidation of pesticides," *Environmental Science & Technology*, vol. 38, no. 13, pp. 3737–3745, 2004.

[6] G. Li Puma and P. L. Yue, "Modelling and design of thin-film slurry photocatalytic reactors for water purification," *Chemical Engineering Science*, vol. 58, no. 11, pp. 2269–2281, 2003.

[7] G. E. Imoberdorf, A. E. Cassano, H. A. Irazoqui, and O. M. Alfano, "Simulation of a multi-annular photocatalytic reactor for degradation of perchloroethylene in air: parametric analysis of radiative energy efficiencies," *Chemical Engineering Science*, vol. 62, no. 4, pp. 1138–1154, 2007.

[8] F. Shiraishi, T. Nomura, S. Yamaguchi, and Y. Ohbuchi, "Rapid removal of trace HCHO from indoor air by an air purifier consisting of a continuous concentrator and photocatalytic reactor and its computer simulation," *Chemical Engineering Journal*, vol. 127, no. 1–3, pp. 157–165, 2007.

[9] S. Romero-Vargas Castrillón and H. I. de Lasa, "Performance evaluation of photocatalytic reactors for air purification using computational fluid dynamics (CFD)," *Industrial and Engineering Chemistry Research*, vol. 46, no. 18, pp. 5867–5880, 2007.

[10] V. Augugliaro, H. Kisch, V. Loddo et al., "Photocatalytic oxidation of aromatic alcohols to aldehydes in aqueous suspension of home prepared titanium dioxide," *Applied Catalysis A: General*, vol. 349, no. 1-2, pp. 189–197, 2008.

[11] S. Higashimoto, N. Kitao, N. Yoshida et al., "Selective photocatalytic oxidation of benzyl alcohol and its derivatives into corresponding aldehydes by molecular oxygen on titanium dioxide under visible light irradiation," *Journal of Catalysis*, vol. 266, no. 2, pp. 279–285, 2009.

[12] N. Qi, H. Zhang, B. Jin, and K. Zhang, "CFD modelling of hydrodynamics and degradation kinetics in an annular slurry photocatalytic reactor for wastewater treatment," *Chemical Engineering Journal*, vol. 172, no. 1, pp. 84–95, 2011.

[13] A. Gora, B. Toepfer, V. Puddu, and G. Li Puma, "Photocatalytic oxidation of herbicides in single-component and multi-component systems: reaction kinetics analysis," *Applied Catalysis B: Environmental*, vol. 65, no. 1-2, pp. 1–10, 2006.

[14] G. Li Puma, "Modeling of thin-film slurry photocatalytic reactors affected by radiation scattering," *Environmental Science & Technology*, vol. 37, no. 24, pp. 5783–5791, 2003.

[15] G. Li puma, "Dimensionless analysis of photocatalytic reactors using suspended solid photocatalysts," *Chemical Engineering Research and Design*, vol. 83, no. 7, pp. 820–826, 2005.

[16] A. Brucato, A. E. Cassano, F. Grisafi, G. Montante, L. Rizzuti, and G. Vella, "Estimating radiant fields in flat heterogeneous photoreactors by the six-flux model," *AICHE Journal*, vol. 52, no. 11, pp. 3882–3890, 2006.

[17] G. Li Puma and A. Brucato, "Dimensionless analysis of slurry photocatalytic reactors using two-flux and six-flux radiation absorption–scattering models," *Catalysis Today*, vol. 122, no. 1-2, pp. 78–90, 2007.

[18] G. Li Puma, V. Puddu, H. K. Tsang, A. Gora, and B. Toepfer, "Photocatalytic oxidation of multicomponent mixtures of estrogens (estrone (E1), 17β-estradiol (E2), 17α-ethynylestradiol (EE2) and estriol (E3)) under UVA and UVC

radiation: photon absorption, quantum yields and rate constants independent of photon absorption," *Applied Catalysis B: Environmental*, vol. 99, no. 3-4, pp. 388–397, 2010.

[19] G. E. Imoberdorf, A. E. Cassano, H. A. Irazoqui, and O. M. Alfano, "Optimal design and modeling of annular photocatalytic wall reactors," *Catalysis Today*, vol. 129, no. 1-2, pp. 118–126, 2007.

[20] V. K. Pareek and A. A. Adesina, "Light intensity distribution in a photocatalytic reactor using finite volume," *AICHE Journal*, vol. 50, no. 6, pp. 1273–1288, 2004.

[21] M. e. M. Zekri and C. Colbeau-Justin, "A mathematical model to describe the photocatalytic reality: what is the probability that a photon does its job?," *Chemical Engineering Journal*, vol. 225, pp. 547–557, 2013.

[22] M. L. Satuf, R. J. Brandi, A. E. Cassano, and O. M. Alfano, "Scaling-up of slurry reactors for the photocatalytic degradation of 4-chlorophenol," *Catalysis Today*, vol. 129, no. 1-2, pp. 110–117, 2007.

[23] M. L. Satuf, R. J. Brandi, A. E. Cassano, and O. M. Alfano, "Modeling of a flat plate, slurry reactor for the photocatalytic degradation of 4-chlorophenol," *International Journal of Chemical Reactor Engineering*, vol. 5, no. 1, 2007.

[24] S. L. Orozco, C. A. Arancibia-Bulnes, and R. Suárez-Parra, "Radiation absorption and degradation of an azo dye in a hybrid photocatalytic reactor," *Chemical Engineering Science*, vol. 64, no. 9, pp. 2173–2185, 2009.

[25] Y. Boyjoo, M. Ang, and V. Pareek, "Light intensity distribution in multi-lamp photocatalytic reactors," *Chemical Engineering Science*, vol. 93, pp. 11–21, 2013.

[26] M. L. Satuf, R. J. Brandi, A. E. Cassano, and O. M. Alfano, "Experimental method to evaluate the optical properties of aqueous titanium dioxide suspensions," *Industrial and Engineering Chemistry Research*, vol. 44, no. 17, pp. 6643–6649, 2005.

[27] G. Sagawe, M. L. Satuf, R. J. Brandi et al., "Analysis of photocatalytic reactors employing the photonic efficiency and the removal efficiency parameters: degradation of radiation absorbing and nonabsorbing pollutants," *Industrial and Engineering Chemistry Research*, vol. 49, no. 15, pp. 6898–6908, 2010.

[28] J. Moreira, B. Serrano, A. Ortiz, and H. de Lasa, "Evaluation of photon absorption in an aqueous TiO_2 slurry reactor using Monte Carlo simulations and macroscopic balance," *Industrial and Engineering Chemistry Research*, vol. 49, no. 21, pp. 10524–10534, 2010.

[29] J. Moreira, B. Serrano, A. Ortiz, and H. de Lasa, "TiO_2 absorption and scattering coefficients using Monte Carlo method and macroscopic balances in a photo-CREC unit," *Chemical Engineering Science*, vol. 66, no. 23, pp. 5813–5821, 2011.

[30] G. L. Puma and P. L. Yue, "A laminar falling film slurry photocatalytic reactor. Part I—model development," *Chemical Engineering Science*, vol. 53, no. 16, pp. 2993–3006, 1998.

[31] L. Hurtado, R. Natividad, E. Torres-García, J. Farias, and G. Li Puma, "Correlating the photocatalytic activity and the optical properties of LiVMoO6 photocatalyst under the UV and the visible region of the solar radiation spectrum," *Chemical Engineering Journal*, vol. 262, pp. 1284–1291, 2015.